NUCLEAR STRUCTURE AND NEUTRINO-NUCLEUS REACTIONS AT SUPERNOVA ENERGIES*

E. YDREFORS, W. ALMOSLY, J. SUHONEN

Department of Physics, University of Jyväskylä,
P. O. Box 35 (YFL), FI-40014 University of Jyväskylä, Finland

Received October 23, 2014

Supernova-(anti-)neutrino–nucleus scattering is discussed with reference to neutral-current (NC) and charged-current (CC) processes in heavy stable nuclei. The Donnelly-Walecka method with the associated multipole expansion of the nucleonic current has been adopted as the basic framework in deriving the neutrino-nucleus scattering cross sections. The needed nuclear wave functions are computed by using the quasiparticle random-phase approximation (QRPA) for the even-even target nuclei in the NC processes and the proton-neutron QRPA (pnQRPA) has been used to compute the CC processes for the mentioned nuclei. The wave functions of the stable odd-mass target nuclei have been obtained by the use of the QRPA-based microscopic quasiparticle-phonon model (MQPM), applied to both NC and CC processes. The obtained cross sections are folded by the energy distributions of the various (anti-)neutrino flavors in order to access detection rates in Earth-based neutrino telescopes. The stable molybdenum (Mo) nuclei serve as examples of application of the formalism, with a subsequent analysis of the results.

Key words: Neutrino-nucleus scattering, supernova neutrinos, neutral-current processes, charged-current processes, quasiparticle random-phase approximation, microscopic quasiparticle-phonon model.

PACS: 21.60.Jz, 25.30.Pt, 23.40.Hc, 27.60.+j.

1. INTRODUCTION

It is well known that supernova neutrinos are very valuable probes of the physics beyond the Standard Model [1, 2] and of the presently poorly known supernova mechanisms [3]. After verification of the non-zero neutrino-mass differences by the neutrino-oscillation experiments the interest in the absolute neutrino mass and the related mass hierarchy has grown substantially. However, the oscillation experiments themselves are not in a position to shed light on the hierarchy problem. Instead, the neutrinoless double beta decays [4–6] can access the absolute mass and hierarchy of neutrinos through the use of the associated nuclear matrix elements [7, 8]. Additionally, the signal produced in a large-scale terrestrial neutrino telescope by a

*Paper presented at the conference "Advanced many-body and statistical methods in mesoscopic systems II", September 1-5, 2014, Brasov, Romania.

future nearby supernova could probably be used to disentangle this important question [9, 10].

From the astrophysical side, nuclear weak interactions play a prominent role during almost all stages of a supernova explosion [11]. Supernovae constitute also one of the proposed sites of the r-process. Neutrino-nucleus reactions would in that case play a leading role for the nucleosynthesis of heavy elements [12].

Neutrinos from astrophysical sources (*e.g.* supernovae or the stars) can be studied by using tonne-scale Earth-bound neutrino telescopes. Examples of existing/planned neutrino detectors are the HALO [13] (lead isotopes), the MOON [14] (molybdenum isotopes), the LAGUNA [15] and possibly the nEXO (^{136}Xe) [16]. Theoretical estimates of neutrino-nucleus cross sections are of paramount importance for the interpretation of the results of such measurements. Nuclear responses to supernova neutrinos constitute also important inputs in supernova simulations.

In this paper we perform a study of the cross sections for the charged-current (CC) and neutral-current (NC) neutrino-nucleus scatterings of the molybdenum isotopes at neutrino energies which are relevant for supernova explosions. Measurable observables are produced by folding the cross sections with realistic energy profiles of the incoming neutrinos.

2. NEUTRAL-CURRENT AND CHARGED-CURRENT SCATTERING

In this work we are interested in the following CC processes

$$\nu_l + (A,Z) \longrightarrow (A,Z+1) + l^-, \tag{1}$$

$$\bar{\nu}_l + (A,Z) \longrightarrow (A,Z-1) + l^+, \tag{2}$$

and the NC processes

$$\nu_l + (A,Z) \longrightarrow (A,Z)^* + \nu_l, \tag{3}$$

$$\bar{\nu}_l + (A,Z) \longrightarrow (A,Z)^* + \bar{\nu}_l, \tag{4}$$

where $l = \mathrm{e}, \mu, \tau$. In the CC reactions (1) and (2) the final nuclear state is either the ground state or an excited state in the nucleus adjacent to the target nucleus. In the incoherent NC reactions (3) and (4) the final nuclear state is an excited state in the target nucleus.

The results that we show here are based on the so-called Donnelly-Walecka formalism [17]. We assume that the involved final and initial nuclear states have well-defined angular momenta and parities and we start from a low-energy effective Hamiltonian with lepton-current–nuclear-current coupling. The nuclear current is then expanded in multipoles leading to nuclear matrix elements containing the nuclear many-body wave functions [18, 19]. Both the lepton and the nuclear current

contain a vector part and an axial-vector part (involving the Pauli spin operator). In addition, the nuclear current contains additional (momentum dependent) vector type and axial-vector type contributions. All these contributions are multiplied by momentum-dependent vector and axial-vector coupling constants [18]. Finally, one can cast the double-differential cross section for the neutrino-nucleus scattering from an initial nuclear state (i) (with angular momentum J_i) to a final nuclear state (f) (with angular momentum J_f) in the form

$$\left(\frac{\mathrm{d}^2\sigma_{i\longrightarrow f}}{\mathrm{d}\Omega\mathrm{d}E_{\mathrm{exc}}}\right)_{\nu/\bar{\nu}} = \frac{G^2|\mathbf{k}'|E_{\mathbf{k}'}}{\pi(2J_i+1)}\Big(\sum_J \sigma^J_{\mathrm{CL}} + \sum_{J\geqslant 1}\sigma^J_{\mathrm{T}}\Big), \tag{5}$$

where $\mathbf{k}$ ($\mathbf{k}'$) is associated to the three-momentum of the incoming (outgoing) lepton and the Coulomb-longitudinal (σ^J_{CL}) and transverse (σ^J_{T}) components are defined in [19]. Here the excitation energy E_{exc} of the final nuclear state is defined with respect to the ground state of the initial nuclear state. For the NC neutrino-nucleus scatterings the effective weak coupling constant is $G = G_{\mathrm{F}}$, where G_{F} denotes the Fermi coupling constant. For the CC processes one has to use $G = \cos\theta_{\mathrm{C}} G_{\mathrm{F}}$, where θ_{C} represents the Cabibbo angle. Additionally, for the CC scattering the expression (5) has to be corrected for the Coulomb distortion of the wave function of the outgoing lepton. We use the methods introduced in [20].

One important quantity from the experimental point of view is the flux-averaged cross section, $\langle\sigma\rangle$, which is computed by folding the cross section $\sigma(E_\nu)$ with an appropriate profile $F_\nu(E_\nu)$ for the energy E_ν of the incoming neutrinos. The energies of supernova neutrinos can rather well be described by a two-parameter Fermi-Dirac distribution

$$\langle\sigma_\nu\rangle = \int \mathrm{d}E_\nu E_\nu^2 F_\nu(E_\nu)\sigma(E_\nu) = \frac{1}{T_\nu^3 F_2(\alpha_\nu)}\int \frac{\mathrm{d}E_\nu E_\nu^2\sigma(E_\nu)}{1+\exp(E_\nu/T_\nu-\alpha_\nu)}, \tag{6}$$

where T_ν is the effective neutrino temperature and α_ν represents the so-called pinching parameter. A similar distribution is valid for anti-neutrinos by replacing ν by $\bar{\nu}$. Here the constant $F_2(\alpha_\nu)$ is chosen such that the total flux is normalized to unity.

In Table 1 are given typical values of the T_ν and α_ν parameters that can be derived from various supernova models (see [21]). The neutrino emission from a supernova core can be regarded as slightly modified black-body radiation. The temperature of the emitted neutrinos depends on their instance of decoupling from the hot star matter. The heavy flavors, ν_μ, ν_τ, and their antiparticles, decouple first at a high temperature as shown in Table 1. The electron neutrinos are the coolest and decouple the last due to their several interactions with the background matter.

Table 1

Typical flavor Fermi-Dirac parameters [21].

Flavor	$\nu_{\rm e}$	$\bar{\nu}_{\rm e}$	ν_μ, ν_τ	$\bar{\nu}_\mu, \bar{\nu}_\tau$
T (MeV)	$2-4$	$4-5$	$6-8$	$6-8$
α_ν	$0-3$	$0-3$	$0-3$	$0-3$

2.1. NUCLEAR MODELS

Here we give a brief review of the nuclear many-body frameworks that are used in the present computations. Both the NC and CC cross-section calculations are always based on a so-called reference nucleus which is an even-even nucleus adjacent to the nuclei involved in the scattering process. For the even-even target nuclei the reference nucleus is the target itself. The excited states in the reference nucleus, used in the NC-scattering calculations, are obtained by using the quasiparticle random-phase approximation (QRPA). For the CC processes one needs the states in the adjacent isobars of the reference and they are thus created by the use of the proton-neutron variant of the QRPA (pnQRPA). These models are treated in detail in [22]. In the case of odd-mass nuclei the wave functions for both the NC and CC processes are calculated by the application of the microscopic quasiparticle-phonon model (MQPM). The MQPM is based on coupling BCS quasiparticles [22] with QRPA phonons of the reference nucleus to produce three-quasiparticle states that mix with one-quasiparticle states through a microscopic residual Hamiltonian. The resulting eigenvalue problem, based on an over-complete non-orthogonal set of basis functions, is solved by the diagonalization of the overlap matrix of the three-quasiparticle states and by a subsequent transformation to the usual hermitian eigenvalue problem (see [23] for details).

In our previous works we have used the Donnelly-Walecka scattering theory and the above-mentioned nuclear many-body frameworks to study the CC and NC neutrino cross sections for the even-even [19, 24] and the odd-mass Mo isotopes [25] by using the Bonn-A G-matrix two-body interactions. In [26] the same interaction was used to study the NC and CC reactions on ^{116}Cd. This target nucleus was also used in [27] to test 10 different Skyrme forces for their CC scattering properties and for their ability to reproduce the relevant spin-isospin features measured in charge-exchange reactions.

3. RESULTS FOR THE STABLE MOLYBDENUM ISOTOPES

The results given in this section for the NC and CC scattering of (anti-)neutrinos off the stable molybdenum isotopes (^{92,94,95,96,97,98,100}Mo) are obtained by using the

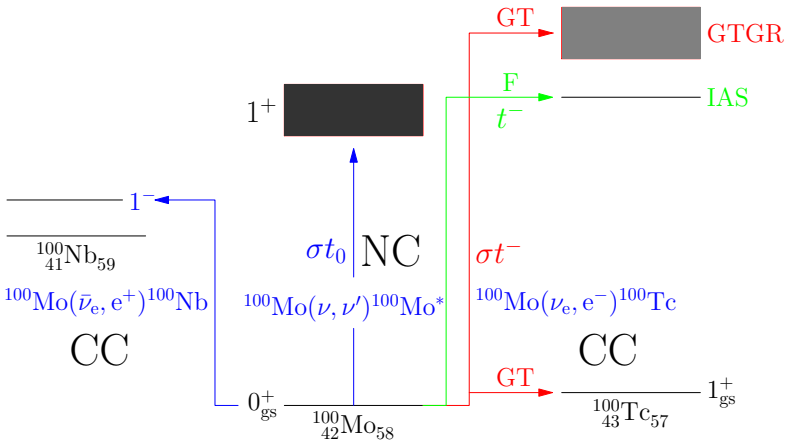

Fig. 1 – Schematic presentation of the charged-current and neutral-current neutrino and anti-neutrino scatterings off ^{100}Mo.

scattering and nuclear-structure formalism presented in the previous sections. Fig. 1 gives a schematic summary of the situation with the NC and CC scatterings using ^{100}Mo as a representative nuclear target. The NC processes lead to excited states of ^{100}Mo and the CC neutrino (anti-neutrino) scatterings lead to states in ^{100}Tc (^{100}Nb).

3.1. NEUTRAL-CURRENT SCATTERINGS

As can be seen in Fig. 1 the NC scatterings (by all the neutrino and anti-neutrino flavors) lead most strongly to the giant spin-flip resonance mediated by the Pauli spin operator. In principle the energy of this resonance could be used to calibrate the QRPA calculations, but unfortunately very little is known experimentally about the location of this resonance.

Fig. 2 presents the results of a large-basis MQPM calculation for the differential NC scattering cross section of an electron neutrino off the nucleus ^{95}Mo. The differential cross section is displayed as a function of the excitation energy in ^{95}Mo. The cross section is normalized by the total cross section such that the sum of the peak heights is unity. As can be seen, the spin excitations at around 6 MeV dominate the cross section through the transitions $5/2^+ \rightarrow 3/2^+, 5/2^+, 7/2^+$ from the $5/2^+$ ground state of ^{95}Mo. Similar dominance of the spin-flip transitions around $6-10$ MeV of excitation is characteristic of the even-even target nuclei as well.

In Fig. 3 the calculated flux-averaged NC electron-neutrino cross sections are displayed for the stable Mo nuclei. There is no drastic dependence on the mass number although a decreasing trend of the cross sections is detectable for the heavy molybdenums. The two odd-mass isotopes stand out with their larger cross sections compared to the ones of even-even isotopes.

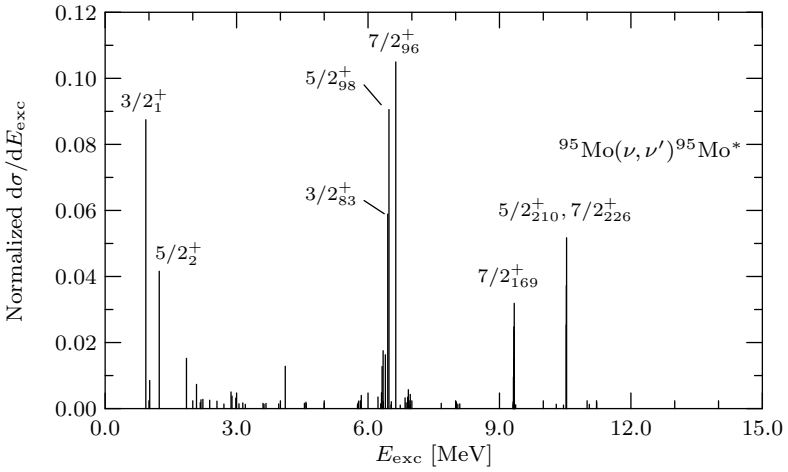

Fig. 2 – NC results for ν_e scattering off ^{95}Mo computed by the MQPM. The numbers to the right of the spin assignments indicate the eigenvalue number after the diagonalizing of the MQPM matrix equations.

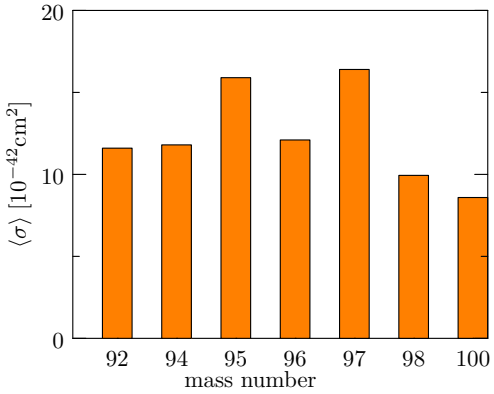

Fig. 3 – Variation of the calculated NC electron-neutrino cross section with mass number for the Mo isotopes.

Finally, in Table 2 we list the computed flux-averaged (anti-)neutrino cross sections for the different neutrino flavors. The mass dependence of the cross sections is qualitatively the same for all flavors. The cross sections for the heavy flavors are larger than for the electron flavor since the kinetic energy (temperature) of the heavy flavors is larger due to their early decoupling from the supernova environment.

Table 2

Flux-averaged incoherent cross sections for the stable molybdenum isotopes in units of $10^{-42}\,\mathrm{cm}^2$

flavor	$\langle\sigma\rangle^{92}$	$\langle\sigma\rangle^{94}$	$\langle\sigma\rangle^{95}$	$\langle\sigma\rangle^{96}$	$\langle\sigma\rangle^{97}$	$\langle\sigma\rangle^{98}$	$\langle\sigma\rangle^{100}$
ν_e	11.6	11.8	15.9	12.1	16.4	9.94	8.59
$\bar{\nu}_\mathrm{e}$	17.3	17.6	23.0	17.9	23.7	15.1	13.1
ν_μ, ν_τ	25.5	25.3	31.5	25.6	32.3	22.1	19.9
$\bar{\nu}_\mu, \bar{\nu}_\tau$	22.7	22.7	28.6	23.0	29.4	20.0	17.7

3.2. CHARGED-CURRENT SCATTERINGS

The charged-current processes are schematically displayed in Fig. 1 for the representative case of scattering off ^{100}Mo. Due to the large muon and tau rest masses only electron neutrinos (or anti-neutrinos) can be detected in neutrino telescopes by using the charged-current reactions (1) and (2). The neutrino reactions lead mostly to the isobaric analogue state (IAS) by a Fermi transition and various 1^+ states through Gamow-Teller transitions. In the latter case the most notable contributions come usually from a few low-lying states and the Gamow-Teller giant resonance and its low-energy satellites (see *e.g.* [27]). The anti-neutrino scattering can lead to a more diverse set of competing multipole states in the final nucleus, like to multipoles $1^-, 1^+, 2^-$.

As mentioned before, only electron (anti-)neutrinos can be detected in the CC scatterings and thus flavor conversion effects in the dense supernova matter begin to play a role. Due to these matter oscillations the initial profile (6) for electron (anti-)neutrinos is modified by the flavor conversions of the heavy flavors, denoted below by ν_x ($\bar{\nu}_\mathrm{x}$). The energy profile for electron (anti-)neutrinos which reach an Earth-bound detector is then given by

$$\begin{aligned} F^{\mathrm{osc}}_{\nu_\mathrm{e}}(E_\nu) &= pF_{\nu_\mathrm{e}}(E_\nu) + (1-p)F_{\nu_\mathrm{x}}(E_\nu); \\ F^{\mathrm{osc}}_{\bar{\nu}_\mathrm{e}}(E_\nu) &= \bar{p}F_{\bar{\nu}_\mathrm{e}}(E_\nu) + (1-\bar{p})F_{\bar{\nu}_\mathrm{x}}(E_\nu), \end{aligned} \tag{7}$$

where F^{osc} denotes the energy profile after the matter oscillations in the exploding star and F are the non-interacting profiles for the electron (anti-)neutrinos and non-electron (anti-)neutrinos, defined in (6). The involved survival probabilities for electron (anti-)neutrinos are given by [28]

$$p = \begin{cases} \sin^2\theta_{13} & \text{Normal hierarchy} \\ \sin^2\theta_{12} & \text{Inverted hierarchy} \end{cases} \qquad \bar{p} = \begin{cases} \cos^2\theta_{12} & \text{Normal hierarchy} \\ \sin^2\theta_{13} & \text{Inverted hierarchy} \end{cases} \tag{8}$$

when no collective neutrino oscillations are included for simplicity. It should be noted that the profiles after the matter oscillations depend on the assumed neutrino mass hierarchy, as shown explicitly in (8).

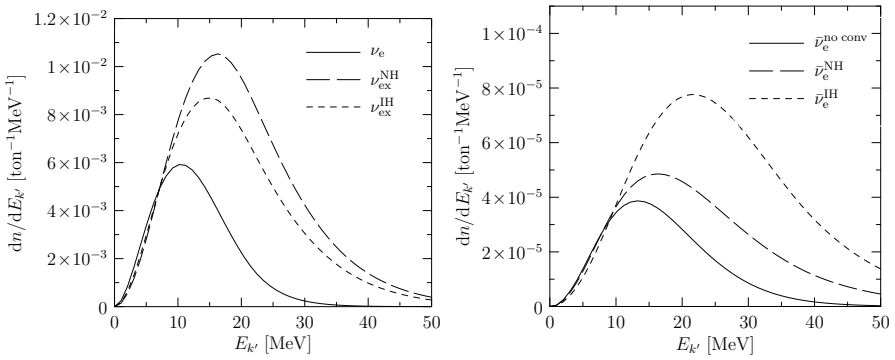

Fig. 4 – Electron (left panel) and positron (right panel) spectra from supernova-(anti-)neutrino CC scattering off ^{100}Mo. Displayed is the number of electrons (positrons) per MeV and kilo-tonne of ^{100}Mo as a function of the energy of the incoming electron (anti-)neutrino.

Fig. 4 presents the results of pnQRPA calculated electron and positron spectra for ^{100}Mo. It is immediately clear that the oscillations increase the number of emitted electron (anti-)neutrinos and thus the number of detected electron (anti-)neutrinos increases in neutrino telescopes. This leads to an increase in the number of emitted electrons (positrons) after the (anti-)neutrino-nucleus interactions in the telescope. Furthermore, for the ν_e induced reactions the difference in the two hierarchies is difficult to observe whereas for the $\bar{\nu}_e$ induced reactions the difference could probably be detected.

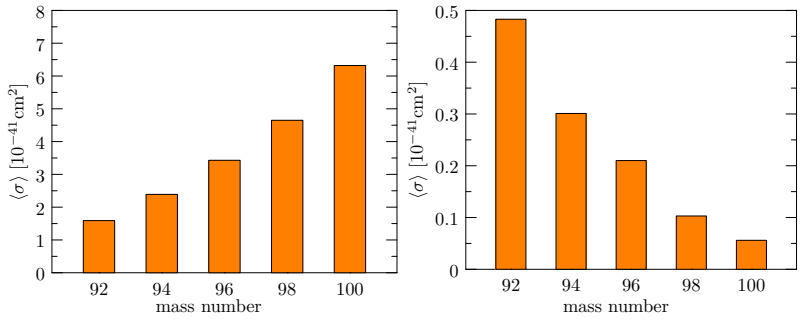

Fig. 5 – Variation of the CC neutrino (left panel) and anti-neutrino (right panel) cross sections with mass number for the Mo isotopes.

Fig. 5 displays the flux-averaged CC scattering cross sections for scatterings off the Mo isotopes separately for the electron neutrinos and anti-neutrinos. There is a clear and opposite trend in the cross sections as functions of the mass number: the neutrino cross sections increase and anti-neutrino cross sections decrease with increasing mass number. The reason for this is displayed in Fig. 6. There are two

effects conspiring to the same direction: (a) the energy-threshold effect and (b) the Pauli-blocking effect. With increasing mass number the energy threshold increases for anti-neutrino scattering and decreases for neutrino scattering leading to a relative increase (decrease) in the neutrino (anti-neutrino) cross sections with increasing mass number. The Pauli blocking shows in the Ikeda $3(N-Z)$ sum rule for Gamow-Teller transitions: the larger the mass number, the larger the sum rule and the (p,n) type of Gamow-Teller transition strength (to the right in Fig. 6) that practically exhausts the sum rule. The reverse happens to the (n,p) type of Gamow-Teller transition strength (to the left in Fig. 6).

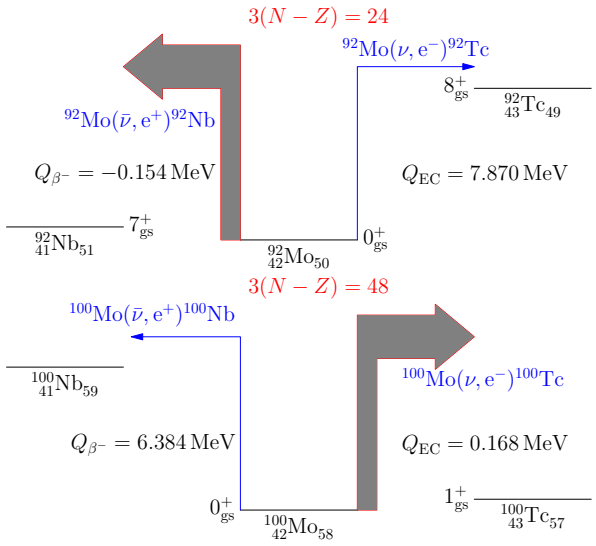

Fig. 6 – Threshold energies and Pauli blocking in the Mo chain of isotopes.

4. CONCLUSIONS

In this work we have performed a study of the charged-current and neutral current (anti-)neutrino-nucleus scatterings off the stable molybdenum isotopes. The cross sections have been computed for supernova-neutrino energies, below 100 MeV. The neutrino-nucleus responses in Earth-bound neutrino telescopes have been computed by folding the cross sections with realistic energy profiles for supernova neutrinos. The nuclear wave functions have been constructed by using the QRPA (NC processes in even-even isotopes) and the pnQRPA (CC processes in even-even isotopes). NC and CC processes in odd-mass isotopes were computed by the use of the QRPA-based MQPM model.

We have found that the CC neutrino and anti-neutrino cross sections are notably modified by the neutrino oscillations in the dense supernova matter. For the supernova scenarios which have been adopted in the present work the CC neutrino cross sections are almost independent of the mass hierarchy. However, the anti-neutrino cross sections differ significantly for the cases of normal/inverted mass hierarchy. In an Earth-bound neutrino telescope most of the events will be caused by CC neutrino scatterings *via* Gamow-Teller transitions. Contrary to this, the anti-neutrinos will mostly cause NC reactions because of the large suppression of the CC anti-neutrino Gamow-Teller channel by the Pauli blocking.

Acknowledgements. This work was supported by the Academy of Finland under the Finnish Center of Excellence Program 2012-2017 (Nuclear and Accelerator Based Program at JYFL).

REFERENCES

1. G. G. Raffelt, Ann. Rev. Nucl. Part. Sci. **49**, 163 (1999).
2. G. G. Raffelt, Prog. Part. Nucl. Phys. **64**, 393 (2010).
3. K. Scholberg, Ann. Rev. Nucl. Part. Sci. **62**, 81 (2008).
4. J. Suhonen, O. Civitarese, Phys. Rep. **300**, 123 (1998).
5. F. T. Avignone III, S. R. Elliott, J. Engel, Rev. Mod. Phys. **80**, 481 (2008).
6. J. Maalampi, J. Suhonen, Adv. High Energy Phys. **2013**, 505874 (2013).
7. J. Suhonen, O. Civitarese, J. Phys. G: Nucl. Part. Phys. **39**, 085105 (2012).
8. J. Suhonen, O. Civitarese, J. Phys. G: Nucl. Part. Phys. **39**, 124005 (2012).
9. A. S. Dighe, J. Phys. Conf. Ser. **136**, 022041 (2008).
10. P. D. Serpico, S. Chakraborty, T. Fisher, L. Hüdepohl, H. T. Janka, A. Mirizzi, Phys. Rev. D **85**, 085031 (2012).
11. K. Langanke, G. Martínez-Pinedo, Rev. Mod. Phys. **75**, 819 (2003).
12. K. Langanke, E. Kolbe, At. Data Nucl. Data Tables **79**, 293 (2001).
13. HALO-Helium and Lead Observatory (http://www.snolab.ca/halo/).
14. H. Ejiri *et al.*, Eur. Phys. J. Special Topics **162**, 239 (2008).
15. LAGUNA-Large Apparatus studying Grand Unification and Neutrino Astrophysics (http://www.laguna-science.eu/).
16. EXO-Enriched Xenon Observatory (https://www-project.slac.stanford.edu/exo/).
17. J. S. O'Connell, T. W. Donnelly, J. D. Valecka, Phys. Rev. C **6**, 719 (1972).
18. E. Ydrefors *et al.*, Nuclear Responses to Supernova Neutrinos for Stable Molybdenum Isotopes, *Neutrinos: Properties, Reactions, Sources and Detection*, ed. J. P. Greene (Nova Science Publishers, 2001).
19. E. Ydrefors, J. Suhonen, Adv. High Energy Phys. **2012**, 373946 (2012).
20. J. Engel, Phys. Rev. C **57**, 2004 (1998).
21. M. T. Keil, G. G. Raffelt, Astrophys. J. **590**, 971 (2003).
22. J. Suhonen, *From Nucleons to Nucleus: Concepts of Microscopic Nuclear Theory* (Springer, Berlin, 2007).
23. J. Toivanen, J. Suhonen, Phys. Rev. C **57**, 1237 (1998).
24. E. Ydrefors, K. G. Balasi, T. S. Kosmas, J. Suhonen, Nucl. Phys. A **896**, 1 (2012).

25. E. Ydrefors, J. Suhonen, Phys. Rev. C **87**, 034314 (2013).
26. W. Almosly, E. Ydrefors, J. Suhonen, J. Phys. G: Nucl. Part. Phys. **40**, 095201 (2013).
27. W. Almosly, B. G. Carlsson, J. Dobaczewski, J. Suhonen, J. Toivanen, P. Vesely, E. Ydrefors, Phys. Rev. C **89**, 024308 (2014).
28. A. S. Dighe, A. Y. Smirnov, Phys. Rev. D **62**, 033007 (2000).